Proceedings of the Institution of Mechanical Engineers Part J: Journal of Engineering Tribology, February 2013, **227**(2):141-153
(Accepted version)

The Influence of Piston Ring Geometry and Topography on Friction

N. Morris[1], R. Rahmani[1*], H. Rahnejat[1], P.D. King[1] and B. Fitzsimons[2]

[1]Wolfson School of Mechanical & Manufacturing Engineering, Loughborough University, Loughborough, UK

[2]Aston Martin Lagonda, Gaydon, Warwickshire, UK

[*]Corresponding author: R.Rahmani@lboro.ac.uk

ABSTRACT

The paper provides solutions for isothermal mixed hydrodynamic conjunction of the compression ring to cylinder liner. This is obtained using the average flow model representation of Reynolds equation based on pressure and shear induced flow factors. In particular the effects of compression ring axial profile along its face-width and surface topography of contiguous solids are investigated. It is shown that ring geometry may be optimized to improve lubrication, whilst care should be taken in order to avoid oil loss or degradation resulting from any loss of sealing. In predicting friction, it is shown that appropriate surface parameters should be used in line with the state of wear of the ring. For a new ring against a plateau honed liner, boundary friction contribution during the initial running-in wear phase should be predicted according to the average asperity peak heights protruding above the plateau, whilst the plateau height also takes into account the valleys within the surface roughness or grooves created by any cross-hatch honing would the appropriate measure of topography for worn rings. The main contributions of the paper are in providing an analytic solution as well investigation of ring face width geometry and effect of wear upon friction. However, it is acknowledged that generated heat, inlet boundary

starvation and circumferential non-conformity of ring to the bore surface would affect the film thickness and exacerbate generated friction accordingly. These further considerations would require a numerical solution, rather than an analytical one presented here.

Keywords: Engines; Piston Rings; Hydrodynamic Friction; Boundary Friction; Surface Roughness

INTRODUCTION

Real surfaces are rough. Therefore, tribological conjunctions with thin lubricating films are invariably subject to the mixed regime of lubrication, where the ubiquitous asperities on the counterfaces play an important role in the flow of lubricant within the contact domain.

Reynolds equation has now been used successfully for more than a century to predict lubricant film thickness and pressure distribution. When the conjunctions are subject to sufficient load, as in counterformal concentrated contacts, combined solution of Reynolds and elasticity potential equation is used to predict the prevailing elastohydrodynamic regime of lubrication (for example, Jalali-Vahid *et al* (1) and Dowson and Ehret (2)). This is the preferred regime of lubrication, when a coherent lubricant film is deemed to guard against the direct interaction of surfaces.

Progressively, thinner lubricant films are encountered for variety of reasons, including down-sizing of machines, increased loading and/or better sealing performance (Dowson (3)). Consequently, mixed regime of lubrication is now prevalent. In fact, as the means of measurement and predictions have improved the realization of dominance of mixed regime of lubrication has become apparent, even retrospectively for many common and long standing conjunctions such as gears (Britton *et al* (4)), cam-followers (Teodorescu *et al* (5)), seals (Nikas

(6)) and of course piston rings (Ma *et al* (7), Akalin and Newaz (8), Bolander and Sadeghi (9) and Mishra *et al* (10) and (11)). This in part has led to the development of models which take into account the effect of surface roughness in tribology, originated by Patir and Cheng (12).

In the past half century, particularly in the study of bio-tribology, it has become evident that mixed regime of lubrication has indeed been the nature's own choice, for example in endo-articular mammalian joints (Dowson and Jin (13)). No longer the tribologists view surface roughness as their nemesis, but in fact a feature which in many cases can be a choice such as laser textured surfaces (Etsion and Sher (14), Rahnejat *et al* (15)). A whole new area of surface engineering has emerged.

Reynolds equation still remains the basis for predictive analysis, but adjusted in order to take into account patterns of flow through rough surfaces (Patir and Cheng (12)). Viscous friction is, therefore, supplemented by contribution made through interaction of asperities or any deliberately introduced surface textures to mitigate conjunctional friction. This has led to more appropriate methods for prediction of friction, for example based on the work of Greenwood and Tripp (16).

For some time now evidence has pointed to the enhanced load carrying capacity of rougher surfaces if boundary regime of lubrication is avoided. In particular, long service life of some fairly rough natural conjunctions, such as articular cartilage and those of common garden slugs became puzzling (Dowson (17)). Then, the hierarchical nature of these tribological conjunctions was noted, in that the invariably *soft* elastohydrodynamic contact contained many localised contact conjunctions, which acted as distributed micro-bearings. The result is pressure perturbations superimposed upon the conjunctional elastohydrodynamic pressures, a

phenomenon referred to as micro-elastohydrodynamics (Gohar and Rahnejat (18)). This realisation has led to engineered surfaces with various feature optimizations, usually in excess of their average surface roughness (Etsion and Sher (14), Rahmani *et al* (19) and (20) and Rahnejat *et al* (15)).

Clearly, surface topography itself as the result of usual machining or fabrication processes follows certain statistical distribution, which has the same effect in fairly thin lubricated contacts. Thus, optimization of lubricated contacts can be carried out with respect to appropriate rough surface parameters. In this paper, the lubrication of piston-ring/cylinder liner conjunction is studied. Patir and Cheng's average flow model (12) is used to represent flow patterns through rough surfaces. Appropriate flow factors are derived by studying surface roughness characteristics. The governing equations are then solved in an analytical manner. Since the flow factors vary locally and are functions of surface profile (through functions of statistical expectancy), the analytical method of solution provides a time efficient approach for optimization of rough ring profiles.

Studies of engine wear patterns, based on surface topography have shown that relatively long term steady-state surface topography can emerge after an initial period of rapid wear termed as 'running-in wear'. In addition, such initial wear may also occur every time during engine cold start. Therefore, for such conditions it may be appropriate to employ more pertinent and indicative surface topography parameters such as Rpk and/or Rk rather than the common Ra (or RMS) parameters. Therefore, the film ratio and the flow factors in the average flow model are altered accordingly in order to ascertain the validity of such hypothesis.

THEORETICAL FORMULATION

Reynolds equation for piston compression ring to cylinder liner contact with an assumed no side leakage of the lubricant becomes:

$$\frac{d}{dx}\left(\frac{h_T^3}{12\eta}\frac{dp}{dx}\right)=\frac{U_1+U_2}{2}\frac{\partial h_T}{\partial x}+\frac{\partial h_T}{\partial t} \qquad [1]$$

The one-dimensional assumed form of Reynolds equation holds for rings whose length exceeds their face-width by a factor of at least 30 as shown by Haddad and Tian (21).

Ma *et al* (7), Akalin and Newaz (8), and Mishra *et al* (10) and (11) have all shown that the generated pressures in the partially conforming ring-liner contact are insufficient to cause any localized contact deformation. Thus, the film shape h_T (average gap) is given as:

$$h_T(x,t)=h(x,t)+\delta_1+\delta_2 \qquad [2]$$

where, $h(x,t)=h_0(t)+S(x)$ is the nominal clearance at any instant of time between the ring face-width and the cylinder wall, $S(x)$ is the local profile of an equivalent solid near a flat plane, $h_0(t)$ is the instantaneous minimum clearance and δ_1 and δ_2 are roughness amplitudes of the contiguous surfaces (Figure 1). The effect of any localised contact elastic deformation is ignored in equation [2]. Previously published works in (7-11) have shown the elastic deformation to be of order of 10^{-8} m. This is particularly true for the type of engine considered in the current analysis. The ring contact face-width is furnished with the hard wear-resistant coating; Ni-Cr-Mo with a modulus of elasticity of 400 GPa. With the maximum contact pressure of 16 MPa no appreciable localised elastic deformation takes place (see Appendix A).

The roughness amplitudes are assumed to follow Gaussian distributions with mean of zero and standard deviations σ_1 and σ_2. Noting that the equivalent solid would be represented by the root mean square of the composite surface roughness, then: $\sigma = \sqrt{\sigma_1^2 + \sigma_2^2}$. Replacing for h_T in Equation [1], letting speed of entraining motion as: $U = \frac{1}{2}(U_1 + U_2)$ and contact factor: $\varphi_c = \frac{dh_T}{dh}$, then:

$$\frac{d}{dx}\left(\frac{\phi_x h^3}{12}\frac{d\overline{p}}{dx}\right) = \eta_0\left(U\phi_c\frac{dh}{dx} + \sigma\frac{\Delta U}{2}\frac{d\phi_s}{dx} + \phi_c\frac{dh}{dt}\right) \quad [3]$$

where the sliding velocity: $\Delta U = U_1 - U_2$.

For the ring-bore conjunction, ignoring any axial flutter or twist motion of the ring, the ring sliding speed: $U_1(\psi) = r\omega\sin\psi\left\{1 + \cos\psi\left[\left(\frac{l}{r}\right)^2 - \sin^2\psi\right]^{-\frac{1}{2}}\right\}$ and the bore surface is stationery: $U_2 = 0$.

Patir and Cheng (12) average flow model is based on Reynolds equation. Equation [3] also assumes iso-viscous incompressible lubricant characteristics. φ_x is the pressure flow factor and φ_s the shear flow factor in the direction of entraining motion *x* (along the axis of the cylinder). These are functions of the Stribeck oil film ratio: $\lambda = h/\sigma$ (see Appendix B). The average pressure is obtained as (Akalin and Newaz (8)):

$$\overline{p} = 6\Delta U\eta_e J_1 + 12\eta_e J_2\frac{\partial h}{\partial t} + C_1 J_3 + C_2 \quad [4]$$

where:

$$J_1 = \int_{-\frac{b}{2}}^{x} \frac{I_1 + \sigma\varphi_s}{\varphi_x h^3} dx, \quad J_2 = \int_{-\frac{b}{2}}^{x} \frac{I_2}{\varphi_x h^3} dx, \quad J_3 = \int_{-\frac{b}{2}}^{x} \frac{1}{\varphi_x h^3} dx \qquad [5]$$

and:

$$I_1 = \int_{-\frac{b}{2}}^{x} \varphi_c \frac{dh}{dx} dx, \quad I_2 = \int_{-\frac{b}{2}}^{x} \varphi_c dx \qquad [6]$$

Boundary Conditions

The inlet boundary condition is set at the edge of the ring at pressure p_{in}. The coordinate system is set such that U_1 always remains positive. Therefore, in the up-stroke motion, p_{in} is the combustion chamber pressure and in the down-stroke, p_{in} is the crank case pressure. Thus:

$$p = p_{in} \text{ at } x = -\frac{b}{2} \qquad [7]$$

This condition assumes that the ring rests on its lower and upper retaining groove lands in down-stroke and up-stroke senses respectively (Perera *et al* (22)). It further assumes a flooded or drowned inlet extending to the edge of the ring face-width at $-b/2$. The exit boundary used in the current analysis is that of Swift (23)-Stieber (24) with an assumed vaporization pressure at the film rupture position:

$$p = p_c, \ \frac{dp}{dx} = 0 \text{ at } x = x_c \qquad [8]$$

Therefore, at the oil rupture position there are three unknowns for the pressure distribution of Equation [4]; C_1, C_2 and x_c. Using the inlet boundary condition in Equation [7], $C_2 = p_{in}$, and using the outlet boundary conditions two expressions are obtained for C_1 whose equality yields:

$$\frac{\left(p_c - p_{in}\right) - 6\eta_e \Delta U J_{1c} - 12\eta_e J_{2c} \dfrac{\partial h}{\partial t}}{J_{3c}} = -6\eta_e \left\{ \Delta U \left(I_{1c} + \sigma \phi_{sc} \right) + 2\dot{h} I_{2c} \right\} \qquad [9]$$

where the integrals *I* and *J* have as their upper limits $x = x_c$. Therefore, the solution to Equation [9] yields the value of x_c. If the value of $x_c > b/2$, then no cavitation occurs and $p = p_{out}$ at $x = b/2$. Other exit boundary conditions have been considered by D'Agostino and Senatore (25).

Friction

As noted in the Introduction, a key consideration in this analysis is the prediction of friction. In Patir and Cheng (26) average flow model, shear stress is a function of flow factors, which are in turn functions of the Stribeck oil film parameter, λ. Hence, the average viscous shear stress becomes:

$$\bar{\tau} = \frac{\eta_0 \Delta U}{h} \left(\phi_f \pm \phi_{fs} \right) \pm \phi_{fp} \frac{h}{2} \frac{\partial \bar{p}}{\partial x} \qquad [10]$$

Thus, viscous friction arising from shear of the lubricant film is obtained as:

$$f_v = 2\pi r_0 \int_{-b/2}^{x_c} \bar{\tau}\, dx \qquad [11]$$

Equation [11] assumes peripheral conformance of the ring to the surface of an idealized right cylindrical bore of radius r_0. In reality the ring does not fully conform to the bore surface, nor is the bore an idealized right circular cylinder. However, this assumption is implicit in the one-dimensional analysis of the contact, as is also the case here.

The regime of lubrication is mixed in the ring-bore conjunction, at least in some parts of the engine cycle, such as at the piston reversal points; at the top and bottom dead centers. In these locations, there is momentary cessation of lubricant entraining motion. Therefore, there is contribution from boundary lubrication caused by asperity interactions on the counterfaces. Boundary friction is obtained as (Greenwood and Tripp (16)):

$$f_b = \tau_0 A_a + \varsigma W_a \qquad [12]$$

where, it is assumed that a thin adsorbed layer of lubricant resides at the asperity summits and acts in accord with non-Newtonian Eyring shear stress τ_0. Additionally, boundary shear strength of surfaces contributes to friction, given by ς. For surfaces with a layer of ferrous oxide: $\varsigma = 0.17$ (Teodorescu *et al* (27)). The asperity contact area A_a and the load share carried by the asperities W_a are functions of typical asperity geometry and their assumed distribution. For a Gaussian distribution these are (Greenwood and Tripp (16)):

$$A_a = \pi^2 \left(\zeta\kappa\sigma\right)^2 AF_2\left(\lambda\right) \qquad [13]$$

$$W_a = \frac{8\sqrt{2}}{15}\pi\left(\zeta\kappa\sigma\right)^2\sqrt{\frac{\sigma}{\kappa}}E'AF_{5/2}\left(\lambda\right) \qquad [14]$$

where $\zeta\kappa\sigma$ is the roughness parameter (Bowden and Tabor (28)), $E^{'}$ is the equivalent plane strain elastic modulus of the counterfaces and the statistical functions are of the form:

$$F_j(\lambda) = \frac{1}{2\pi}\int_{\lambda}^{\infty}(s-\lambda)^j \exp\left(-\frac{s^2}{2}\right)ds \qquad [15]$$

Thus, the overall friction is obtained as:

$$f = f_v + f_b \qquad [16]$$

METHOD OF SOLUTION

At any crank angle ψ, a load balance condition is sought:

$$\left|\frac{W_h + W_a - F}{F}\right| \le \varepsilon \qquad [17]$$

where, in the current study: $\varepsilon = 10^{-4}$. The parameter F is the outward force acting on the ring's inner rim, striving to adhere it to the bore surface. It comprises the ring tension force, as well as the gas pressure acting behind the ring (Ma *et al* (7) and Mishra *et al* (10)). Thus:

$$F = \left(p_e + p_g\right)br_0 \qquad [18]$$

p_e is a uniform elastic pressure, given as (Bin Chik and Fessler (29)):

$$p_e = \frac{gEI}{3\pi br_0^4} \qquad [19]$$

where, for the ring cross-section: $I = bd^3/12$.

The elastic pressure arises as the result of fitment of an incomplete circular ring, having an end gap of g prior to fitment, typically of several millimeters, into a smaller bore of nominal radius r_0 . Equation [19] assumes that the back of the top compression ring is exposed to the combustion chamber pressure. In practice, the ring undergoes complex motions and, therefore, the gas pressure behind the ring alters in a complex manner. For quasi-static equilibrium the inertial and flexural motions of the ring are ignored, thus an instantaneous balance between the applied load *F* and the contact reaction due to the generated hydrodynamic and asperity pressures is sought, where:

$$W_h = 2\pi r_0 \int_{-b/2}^{x_c} p\,dx \qquad [20]$$

The asperity load share is given by Equation [13]. Therefore, the solution procedure requires simultaneous solution of Equations [2] and [3], satisfying the convergence criterion in Equation [17]. If this condition is not met, the instantaneous minimum clearance h_0 is altered and the calculation procedure is repeated:

$$h_0^k = (1+\beta\chi)\,h_0^{k-1} \qquad [21]$$

χ is an adjusting parameter: $\chi = \dfrac{(W_h + W_a) - F}{\max\{(W_h + W_a), F\}}$. The superscript k denotes the iteration steps. A damping coefficient $\beta = 0.005$ was used to produce faster load convergence, whilst avoiding numerical instability in the convergence process.

When the convergence criterion is met the crank-angle ψ is advanced, the new sliding velocity of the ring is obtained and the entire calculation procedure is repeated.

RESULTS AND DISCUSSION

The case considered in this analysis is a typical compression ring of a V12 engine. Table 1 provides the data used in the analysis. The results presented here are for the engine speed of 4000 rpm. The combustion curve at this speed is shown in Figure 2.

The axial profile of the ring along its face-width plays an important role in the entrainment of the lubricant into the conjunction through the inlet wedge effect. A larger wedge angle increases the flow rate and the film thickness for a given sliding speed, but reduces the generated contact pressures, thus the load carrying capacity. Additionally, larger wedge angles in flow rates can result in oil loss and hence sealing (Nikas (6)), which is the primary function of the compression ring. Conversely, rings with larger effective radius of curvature represent shallower wedge angles, resulting in lower rate of lubricant entrainment and thinner films which can increase boundary friction. The ring axial profile may be approximated by:

$$S(x) = \frac{h_c x^n}{(b/2)^2} \qquad [22]$$

where, the effective radius of curvature is: $R = \frac{b^2}{8h_c}$.

Therefore, it is important to determine the optimum axial profile of the ring. A preliminary study is carried out with value of $1.8 \le n \le 2.4$ (Figure 3). Note that most studies approximate the ring profile to a parabola or $n = 2$ (D'Agostino and Senatore (25), Mishra *et al* (10) and (11) and Ma

et al (7)). This rather idealised parabolic ring face-width profile is retained in the current analyses because of various results in literature, against which the more realistic worn profiles are benchmarked.

Film thickness variation for different values of *n* is shown in Figure 4. It can be observed that a parabolic axial ring face-width profile consistently provides a thicker film than other alternatives. Therefore, it may be conceived that a parabolic profile is the optimum as there would be least likelihood of mixed or boundary regimes of lubrication ($\lambda < 3$).

Figure 5 shows the predicted friction for different ring profiles. The parabolic ring profile, promoting the formation of a thicker film has a higher viscous load carrying capacity. One would then expect reduced viscous friction, which dominates for most of the engine cycle. This is also in line with the well-known inverse relationship between viscous shear stress and film thickness; $\tau_v \propto \frac{\Delta U \eta_0}{h}$. This is certainly the case for values of $n \geq 2$ in Figure 5. However, higher inlet wedge angles also promote larger changes in the pressure gradient $\frac{\partial p}{\partial x}$ and consequently pressure induced shear in Equation [10] becomes comparable with that due to lubricant film shear itself. Hence, any optimization of the ring profile should take into account that for rings with a high crown height pressure-induced shear can be quite significant. Of course in practice, compression ring's edge profiles are not symmetrical, thus a profile-function of the type usually assumed in the predictive analysis (also in Figures 4 and 5) is rather idealistic. In fact, the wedge angle at the upper edge of the compression ring is usually larger than that at its lower face (Figure 6). Therefore, in the down-stroke motion it presents a diverging gap so that ideally the pressure-induced shear would exceed that due to the sliding motion. This would ensure

cavitation of the lubricant just prior to the ring upper edge and hence maintain its sealing effectiveness (Nikas (6)). In the upstroke motion, where in practice a meniscus of lubricant on the usually hot chamber surface hardly exists, a large pressure gradient imposed by the higher ring crown height inhibits the flow of combustion gasses into the ring pack. Thus, any film of lubricant would be thinner, for example, in the transition from compression to the power stroke. Here, a larger wedge angle also serves the purpose of increasing the gap between the contiguous surfaces in order to mitigate wear by direct boundary interactions.

Before proceeding to the case of an actual ring geometry, it is important to note that flow of lubricant through the ring-pack is an important consideration from the points of view of lubrication and sealing. These two requirements are often contradictory in nature. For the case of rings with various values of n, Figure 7 shows the mass flow rate of the lubricant through the minimum film constriction. As expected with the larger values of n, a higher converging-diverging profile results which facilitates a greater mass flow rate, if a fully flooded inlet is assumed, as is the case in this analysis. Comparison of this with Figure 5 for the cases of n =1.8 and n=2 shows the contradictory requirements in mitigating friction with that of the ring sealing function. It also shows the reason for choosing an asymmetrical ring face-width profile, which is usually arrived at through experience rather than by any analytical rigor.

Now returning to the case of actual rather than idealized ring face-width profile, shown in Figure 6, it is clear that boundary interactions at the dead centres or in their immediate vicinity, as well as elsewhere due to any bore out-of-roundness can lead to wear. The figure also shows the extreme case of a worn ring profile after its useful life has elapsed. This represents the ring profile after accelerated engine testing, representing a typical 150,000 miles usage. It is

noteworthy that the severely worn wedges would reduce the chance of lubricant entrainment into the conjunction.

Figure 8 shows that both the new and worn actual ring profiles promote slightly thinner films than the idealized parabolic profile; n =2. The difference, however, is quite small, even between the significantly worn ring and the new. All the profiles also show very thin films at the TDC, in transition from the compression to the power stroke, indicating that mixed or boundary regimes of lubrication would be prevalent. Traditionally, the composite root mean square (RMS) roughness of the counterface surfaces ($\sigma = \sqrt{R_{a1}^2 + R_{a2}^2}$) is used to ascertain the regime of lubrication. However, the composite surface R_a is not a good indication of either initial wear or the usually plateau honed surface of cylinder liners. Its value can be the same for surfaces of quite different topography as it represents the average of topographical features. Figure 9 shows this anomaly, where the total friction based on RMS is used. Hardly, a change is noted between the total friction (viscous and boundary) between the same three rings, subject of analysis in Figure 8. This is because at the transition from the compression to power stroke, boundary friction is significant and R_a is not representative of different stages of the wear process. Elsewhere, viscous friction dominates and film thickness for all the three cases is almost the same (Figure 8). It is intuitive that in practice these observations would not be upheld. The initial wear in the compression ring-cylinder liner conjunction is dominated by the asperity peaks protruding above the plateau of a cross-hatched honed liner surface (Gore *et al* (31)). These are best represented by the statistical parameter R_{pk}^* which represents the average height of these peaks. The period of initial wear varies from engine to engine and depends on the duty cycle. It can typically last for several thousand miles. Gore *et al* (31) show that a plateau is then formed,

even if no cross-hatch honing is carried out, whose average height is determined by any small residual protruding peaks and the valleys of the topography. The height of plateau varies as a moving average during the gradual wear process, and is represented by the statistical parameter R_k. All the approaches used, based on the surface roughness parameters clearly assume a statistical distribution of asperities. These include the average flow model, initially developed by Patir and Cheng (12, 26). It is, however, noted by other authors such as Michail and Barber (32) and Spencer *et al* (33) that the topography of cross-hatched plateaued surfaces does not follow a Gaussian distribution. These authors have derived alternative simple equations to represent the plateau surface instead of using the more widely used average flow model. Other recent approaches, for example by Komvopoulos (34) make use of scale-independent fractal representation, which may be suitable for small representative contact areas. The study of wear by Gore *et al* (31) shows that the wear of cross-hatch honed surfaces changes the distribution of peaks R_{pk^*} during the running-in wear and because of the small portion of peaks it hardly affects the platform height R_k. During gradual wear and embedding of surfaces Gore *et al* (31) show insignificant wear of cross-hatch valleys, whilst the platform wear affects the R_k value. Therefore, the approach used here is based on the experimental evidence presented by Gore *et al* (31).

Table 1 lists the measured surface parameters using optical Talysurf profilometer for the new and the worn rings used in the current study. Note the variation of the R_k value. Therefore, representative prediction of friction, particularly at the TDC reversal depends, not only on the state of ring geometry but also on its surface topography. For a new ring, the assessment of friction should be based on its asperity peaks, represented by R^*_{pk} and during the initial wear

process. Thereafter, the appropriate measure for boundary contribution to friction should be based on the R_k parameter. Figure 10 shows the results of such analyses.

It can be observed that the significant differences occur in the region corresponding to the transition from the compression to the power stroke and extending just beyond the point of maximum combustion pressure (the detonation point), denoted by the crank-angle position of 20° for the engine, subject of the current analysis. The difference between the new ring's friction based on R_{pk}^{*} and that for the worn one, using the R_k parameter are representative of ring life time friction performance. Note that the area enclosed between these two curves represents the frictional power losses of a new ring in excess of a run-in worn ring, which gradually reduces during its useful life. Although this power loss looks small in Figure 10, one should remember that this accounts for just one engine cycle, and at 4000 rpm (this case). In excess of 65 such cycles are encountered every second. Therefore, as the friction at the TDC is reduced during the initial and gradual wear processes frictional power loss is reduced at the expense of an increasing ring-bore gap (Figure 8) which can lead to loss of ring sealing, oil loss and degradation.

CONCLUSIONS

Analysis of compression ring-cylinder liner conjunction is quite complex on the account of the transient nature of regime of lubrication, caused by large variations in contact kinematics, reversals at the dead centres and significant changes in the contact load during an engine cycle. In particular, the compression ring has a number of functions, chiefly sealing of the combustion chamber and transfer of heat away from its conjunction (not tackled in the current isothermal analysis). These requirements often conflict with the need to reduce engine parasitic losses, dominated by friction, in order to improve fuel efficiency which is the key driver in engine

development. Hence, it is necessary to be able to analyse ring geometry in a process of optimization. This is the primary purpose and contribution of the current analysis. The paper shows that the contradictory requirements set for the compression ring functional performance makes this process quite hard, and an optimal solution should take into account friction, lubricant flow rate and ring geometry. It is also shown that prediction of ring frictional performance requires proper description of its topography as a function of various stages of wear. Ring reversal at the TDC promotes significant boundary friction contribution which must be predicted with suitable topographical parameters. Figure 11 shows that the commonly used *Ra* parameter leads to significant misrepresentation of prevailing conditions.

Finally, it is noteworthy that the analysis reported here is isothermal, which leads to an over-estimation of the lubricant film thickness, as the heat generated in the contact alters the viscosity of the lubricant and further reduces the film thickness. Another assumption made in the current analysis is fully flooded inlet condition. In practice, the contact inlet may well be starved, thus leading to further diminution of the film thickness. The current analysis also treats the ring-bore conjunction in one dimension along the ring face-width, implying good circumferential ring-bore conformance. In practice there is significant non-conformity due to bore out-of-roundness and ring elastodynamics. The plethora of such salient practical features demonstrates the complexity of the compression ring conjunction and provides the motivation for the future extensions of this research. However, the current paper provides an analytic solution to the problem which is computationally less intensive and more in line with industrial time scales.

ACKNOWLEDGMENT

The authors would like to express their gratitude to the Engineering and Physical Sciences Research Council (EPSRC) for the sponsorship of this research under the Encyclopaedic Program Grant (www.Encyclopaedic.org). Thanks are also extended to the other partner organisations, particularly in this instance to Aston Martin Lagonda for both its financial and technical support.

REFERENCES

(1) Jalali-Vahid, D., Rahnejat, H., Gohar, R. and Jin, Z.M. (1998), "Comparison between experiments and numerical solutions for isothermal elastohydrodynamic point contacts," *J. Phys., D: Appl. Phys.* **31**, pp. 2725-2732.

(2) Dowson, D. and Ehret, P. (1999), "Past, present and future studies in elastohydrodynamics," *Proc. IMechE, Part J: Engng. Trib.* **213**, pp. 317-333.

(3) Dowson, D. (1992),"Developments in lubrication- the thinning film," *J. Phys., D: Appl. Phys.* **25**, pp. 334-339.

(4) Britton, R.D., Elcoate, C.D., Alanou, M.P. and Snidle, R.W. (2000), "Effect of Surface Finish on Gear Tooth Friction," *Trans. ASME, J. Trib.* **122**, pp. 354-360.

(5) Teodorescu, M., Kushwaha, M., Rahnejat, H. and Taraza, D. (2005), "Elastodynamic transient analysis of a four-cylinder valvetrain system with camshaft flexibility," *Proc. Instn. Mech. Engrs., Part K: J. Multi-body Dyn.* **219**, pp. 13-25.

(6) Nikas, G.K. (2003), "Transient elastohydrodynamic lubrication of rectangular elastomeric seals for linear hydraulic actuators," *Proc. Instn. Mech. Engrs. Part J: J. Engng. Trib.* **217**, pp. 461-473.

(7) Ma, M.-T., Sherrington, I. and Smith, E.H. (1997), "Analysis of lubrication and friction for a complete piston-ring pack with an improved oil availability model – Part 1: circumferentially uniform film," *Proc. IMechE, Part J: J. Engng. Trib.* **211**, pp. 1-15.

(8) Akalin, O. and Newaz, G.M. (2001), "Piston ring-cylinder bore friction modeling in mixed lubrication regime: Part I—Analytical results," *Trans. ASME, J. Trib.* **123**, pp. 211-218.

(9) Bolander, N.W. and Sadeghi, F. (2007), "Deterministic Modeling of Honed Cylinder Liner Friction," *Trib. Trans.* **50**, pp. 248-256.

(10) Mishra, P.C., Balakrishnan, S. and Rahnejat, H. (2008), "Tribology of compression ring-to-cylinder contact at reversal," *Proc. IMechE, Part J: J. Engng. Trib.* **222**, pp. 815-826.

(11) Mishra, P.C., Rahnejat, H. and King, P.D. (2009), "Tribology of the ring-bore conjunction subject to a mixed regime of lubrication," *Proc. IMechE, Part C: J. Mech. Engng. Sci.* **223**, pp. 987-998.

(12) Patir, N. and Cheng, H.S. (1978), "An average flow model for determining effects of three-dimensional roughness on partial hydrodynamic lubrication," *Trans. ASME, Series F: J. Lubn. Tech.* **100**, pp. 12-17.

(13) Dowson, D. and Jin, Z.M. (1986), "Micro-elastohydrodynamic lubrication of synovial joints," *Proc. IMechE, Part H: J. Engng. In Medicine*, **15**, pp. 63-65.

(14) Etsion, I. and Sher, (2009), "Improving fuel efficiency with laser surface textured piston rings," *Trib. Int.* **42**, pp. 542-547.

(15) Rahnejat, H., Balakrishnan, S., King, P.D. and Howell-Smith, S. (2006), "In-cylinder friction reduction using a surface finish optimization technique," *Proc. IMechE, Part D: J. Auto. Engng.* **220**, pp. 1309-1318.

(16) Greenwood, J.A. and Tripp, J.H. (1970-1971), "The contact of two nominally flat rough surfaces," *Proc. IMechE.* **185**, pp. 625-634.

(17) Dowson, D. (2009), "A tribological day," *Proc. IMechE, Part C: J. Mech. Engng. Sci.* **223**, pp. 261-273.

(18) Gohar, R. and Rahnejat, H. (2008) "Fundamentals of tribology," Imperial College Press., London, UK, ISBN-10 978-1-84816-184-9

(19) Rahmani, R., Shirvani, A. and Shirvani, H. (2007), "Optimization of Partially Textured Parallel Thrust Bearings with Square-Shaped Micro-Dimples," *Trib. Trans.*, **50** (3), pp. 401-406

(20) Rahmani, R., Shirvani, A. and Shirvani, H. (2010), "Optimised textured surfaces with application in piston-ring/cylinder liner contact," Chapter 14 in Rahnejat, H. (Ed.) "Tribology and dynamics of engine and powertrain: Fundamentals, applications and future trends", *Woodhead Publishing, Cambridge, UK*.

(21) Haddad, S.D. and Tian, K-T. (1995), "Analytical study of offset piston and crankshaft designs and the effect of oil film on piston slap excitation in a diesel engine," *Mech. Mach. Theory.* **30**, pp. *271-284.*

(22) Perera, M. S. M., Theodossiades, S. and Rahnejat, H. (2010) "Elasto-multi-body dynamics of internal combustion engines with tribological conjunctions," *Proc. IMechE, Part K: J. Multi-body Dyn*. **224**, pp. 261-277.

(23) Stieber, W. (1933) "Dus Schwimmlager," *Verein Deutscher Ingenieurre, Berlin.*

(24) Swift, H. W. (1932), "The stability of lubricating films in journal bearings," *J. Inst. Civ. Engrs.* **233**, *Part l, pp. 267.*

(25) D'Agostino, V. and Senatore, A. (2010), "Fundamentals of lubrication and friction of piston ring contact," in: Rahnejat, H. (ed.), "Tribology and dynamics of engine and powertrain", *Woodhead Publishing*, Cambridge, UK, pp.343-384.

(26) Patir, N. and Cheng, H.S. (1979), "Application of Average Flow Model to Lubrication between Rough Sliding Surfaces," *Trans. ASME, Series F: J. Lubn. Tech.* **101**, pp. 220-230.

(27) Teodorescu, M., Kushwaha, M., Rahnejat, H. and Rothberg, S.J. (2007), "Multi-physics analysis of valve train systems: from system level to microscale interactions," *Proc. IMechE, Part K: J. Multi-body Dyn.* **221**, pp. 349-360.

(28) Bowden, F.P., Tabor, D. (2001), "The Friction and Lubrication of Solids," Clarendon Press, Oxford, UK, ISBN 10 0198507 77.

(29) Bin Chik, A. and Fessler, H. (1966), "Radial pressure exerted by piston rings," *J. Strain Anal., I (2),* pp. *165-171.*

(30) Chengwei, W. and Linqing, Z. (1989), "An average Reynolds equation for partial film lubrication with a contact factor," *Trans. ASME, J. Trib.* **111**, pp. 188-191.

(31) Gore, M., Perera, M., Styles, G., King, P.D. and Rahnejat, H. (2011), "Wear characteristics of advanced honed and cross-hatched coated cylinder liners", Proc. *66th annual meeting and Exhibition of the STLE, Atlanta, Georgia, May 2011, pp.* 73

(32) Michail, S.K. and Barber, G.C., (1995), "The Effects of Roughness on Piston Ring Lubrication—Part I: Model Development", *Tribology Transactions*, **38**, pp. 19-26

(33) Spencer, A., Almqvist, A. and Larsson, R. (2011), "A numerical model to investigate the effect of honing angle on the hydrodynamic lubrication between a combustion engine piston ring and cylinder liner", *Proc IMechE, Part J: J. Engng. Trib.*, **225**, pp. 683-689

(34) Komvopoulos, K. (1996), "Surface engineering and microtribology for microelectromechanical systems", *Wear*, **200**, pp. 305-327

(35) Rahnejat, H. (2000) "Multi-body dynamics: historical evolution and application", *Proc. IMechE, Part C: J. Mech. Engng. Sci.*, **214**, pp. 149-173

APPDENIX A

With hard wear resistant coating; Ni-Cr-Mo provided on the contact face-width of the ring, a simple calculation confirms insignificant localised deformation of its surface under the pressures generated. For simplicity a column method approach (35) is employed, where:

$$\delta = \frac{(1-2\upsilon)(1+\upsilon)d}{E(1-\upsilon)}p \qquad \text{(A.1)}$$

where, υ is the Poisson ratio, E is Young's modulus of elasticity, d is ring thickness and p is the maximum generated pressure. The maximum pressure in the contact, for the studied engine, is around 16MPa at detonation point (maximum combustion pressure). The ring coating is Ni-Cr-Mo with typical mechanical properties of E=400GPa and υ=0.2 is used and typically d=3mm, then the resulted deformation would be: $\delta = 0.011\ \mu$m, whilst the minimum film thickness at this point obtained as 1.04μm.

APPENDIX B

The flow factors used are described below:

The pressure flow factor φ_x is calculated using an empirical relationship, shown by Patir and Cheng (11) as:

$$\varphi_x = 1 - 0.9e^{-0.56\lambda},\ \lambda > 0.5 \text{ and } \gamma = 1 \qquad \text{(B.1)}$$

where γ is the ratio of correlation lengths in the *x* and *y* directions of the contact solids as described in (11). It distinguishes between the various patterns of surface roughness. If an isotropic roughness is assumed, as in the current case, then clearly: $\gamma = 1$.

The shear flow factor is calculated using another empirical relationship stated as (24):

$$\varphi_s = \begin{cases} 1.899\lambda^{0.98}\left(V_1 - V_2\right)e^{\left(-0.92\lambda + 0.05\lambda^2\right)} & , \lambda \le 5,\ \gamma = 1 \\ 1.126\left(V_1 - V_2\right)e^{-0.25\lambda} & , \lambda > 5,\ \gamma = 1 \end{cases} \quad \text{(B.2)}$$

Where V_1 and V_2 are the variance ratios $V_i = \dfrac{\sigma_i^2}{\sigma^2},\ i \in 1,2$

The contact factor for a partially lubricated conjunction is given as (28):

$$\varphi_c = \frac{1}{2}\left[1 + erf\left(\lambda\right)\right] \quad \text{(B.3)}$$

The shear stress factors; φ_{fp}, φ_{fs} and φ_f are given in (24) as:

$$\varphi_{fp} = 1 - 1.4e^{-0.66\lambda} \quad , \lambda > 0.75,\ \gamma = 1 \quad \text{(B.4)}$$

$$\varphi_{fs} = \begin{cases} 11.1\lambda^{2.31}\left(V_1 - V_2\right)e^{\left(2.38\lambda + 0.11\lambda^2\right)} & , 0.5 < \lambda < 7,\ \gamma = 1 \\ 0 & , \lambda > 7 \end{cases} \quad \text{(B.5)}$$

and:

$$\varphi_f = \begin{cases} \frac{35}{32}\xi\left\{\left(1-\xi^2\right)^3 \ln\left[300\left(1+\xi\right)\right]+\frac{1}{60}N\right\} & ,\ \lambda \le 3 \\ \frac{35}{32}\xi\left\{\left(1-\xi^2\right)^3 \ln\left(\frac{\xi+1}{\xi-1}\right)+\frac{\xi}{15}\left[66+\xi^2\left(30\xi^2-80\right)\right]\right\} & ,\ \lambda > 3 \end{cases} \quad \text{(B.6)}$$

where: $\xi = \lambda/3$ and:

$$N = \xi\left\{\xi\left[132+\xi\left(M+345\right)\right]\right\}-55 \quad \text{and} \quad M = \xi\left\{\xi\left[\xi\left(60+147\xi\right)-405\right]-160\right\}$$

NOMENCLATURE

A	Apparent contact area
A_a	Asperity contact area
A_h	Hydrodynamic contact area
b	Ring face-width
d	Ring radial width (thickness)
E	Reduced (effective) elastic modulus of the contacting pair
F	Total external load on the ring
f	Total friction
f_e	Ring elastic force
f_g	Gas force acting behind the ring
f_b	Boundary friction
f_v	Viscous friction
g	Incomplete circular rings free end gap (pre-fitment)
h	Film thickness

h_0	Minimum film thickness
h_T	Rough surface film thickness
l	Ring length or bore perimeter
n	Ring profile parameter
p	Pressure
$\bar{p}$	Average pressure
p_c	Cavitation vaporization pressure
p_e	Ring elastic pressure due to fitment
p_g	Gas pressure acting behind the ring
p_{in}	Inlet pressure
p_{out}	Outlet pressure
r	Crank-pin radius
r_o	Nominal bore radius
R	Ring radius
S	Profile of the ring face-width
t	Time
U	Speed of entraining motion
V	Variance ratios of rough surfaces
W_a	Load share of asperities
x	Direction along the ring face-width (direction of entraining motion)
x_c	Film rupture boundary

Greek Symbols

β	Damping coefficient

δ_1, δ_2	Roughness amplitude on the bore and ring surfaces
ΔU	Sliding velocity
ε	load convergence criterion
φ_c	Contact factor
φ_f , φ_{fs}, φ_{fp}	Friction-induced flow factors
φ_s	Shear flow factor
φ_x	Pressure flow factor
γ	Surface roughness orientation parameter
η_0	Lubricant dynamic viscosity at atmospheric pressure and ambient temperature
κ	Average asperity tip radius
λ	Stribeck oil film parameter
χ	Load balance parameter
ρ	Lubricant density
σ_1, σ_2	Roughness *Ra* or R_k of liner and ring
σ	Root mean square roughness of contiguous surfaces
ς	Boundary shear strength of surfaces
$\bar{\tau}$	Average shear stress
τ_0	Eyring shear stress of lubricant
ω	Engine speed
ζ	Asperity density per unit contact area
ψ	Crank angle

Table Captions

Table1: Engine conditions

Figure Captions

Figure 1: Film thickness function

Figure 2: In-cylinder pressure variation during the whole engine cycle at 4000 rpm

Figure 3: Various approximated ring axial profiles

Figure 4: Variations of minimum film thickness for different ring profiles during a typical engine cycle

Figure 5: Variations of total friction force for different ring profiles during a typical engine cycle

Figure 6: Typical new and worn (end of the life cycle) ring profiles

Figure 7: Variations of lubricant mass flow rate for different ring profiles during a typical engine cycle

Figure 8: Variation of minimum film thickness for various rings

Figure 9: Total viscous and boundary friction based on composite Ra values

Figure 10: Total friction force: viscous and boundary

Figure 11: Asperity friction force for near TDC

Tables

Table1: Engine conditions

Parameter	Value	Unit
Crank radius	79.5	*mm*
Connecting rod length	138.1	*mm*
Bore radius	44.52	*mm*
Bore surface roughness (Ra)	0.26	μm
New ring surface roughness (Ra, Rpk*, Rk)	0.408,0.996,1.32	μm
Worn ring surface roughness (Ra, Rk)	0.235,0.585	μm
Ring face-width	1.2	*mm*
Lubricant viscosity	0.05 (at 40°C)	*Pa.s*
Engine speed	4000	*rpm*

Figures

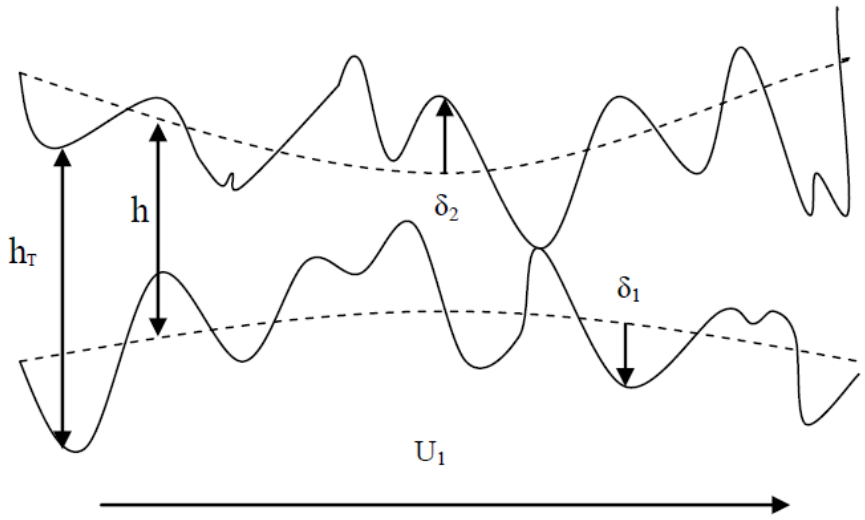

Figure 1: Film Thickness Function

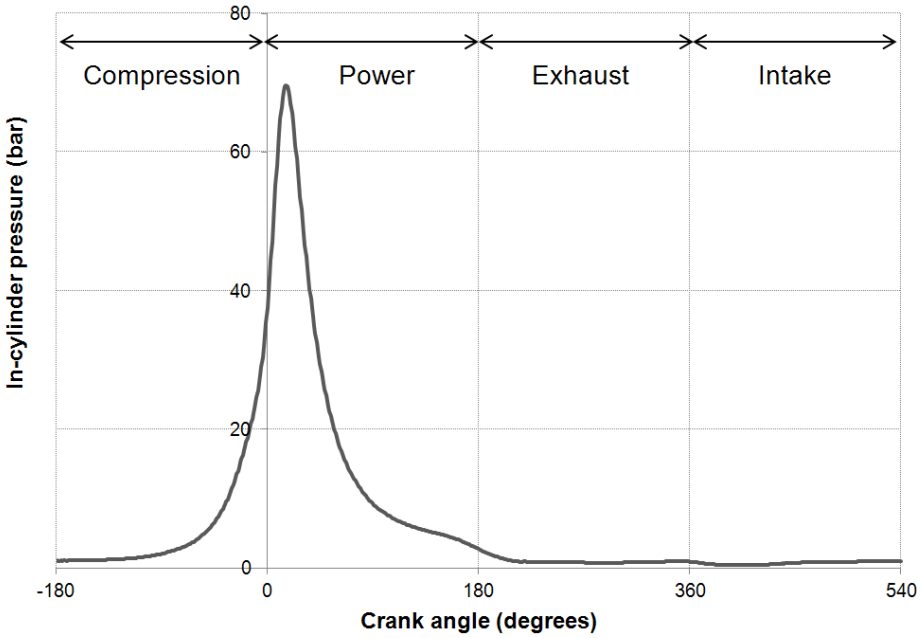

Figure 2: In-cylinder pressure variation during the whole engine cycle at 4000 rpm

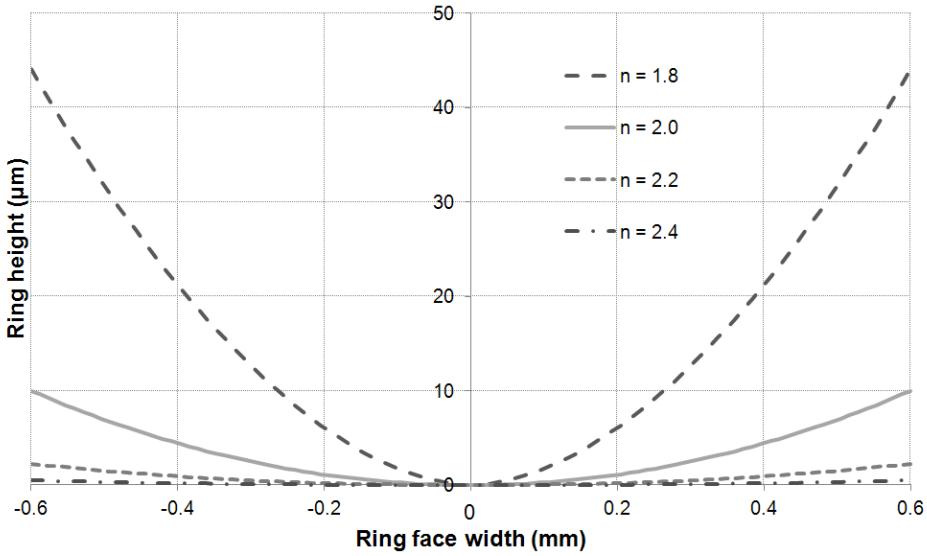

Figure 3: Various approximated ring axial profiles

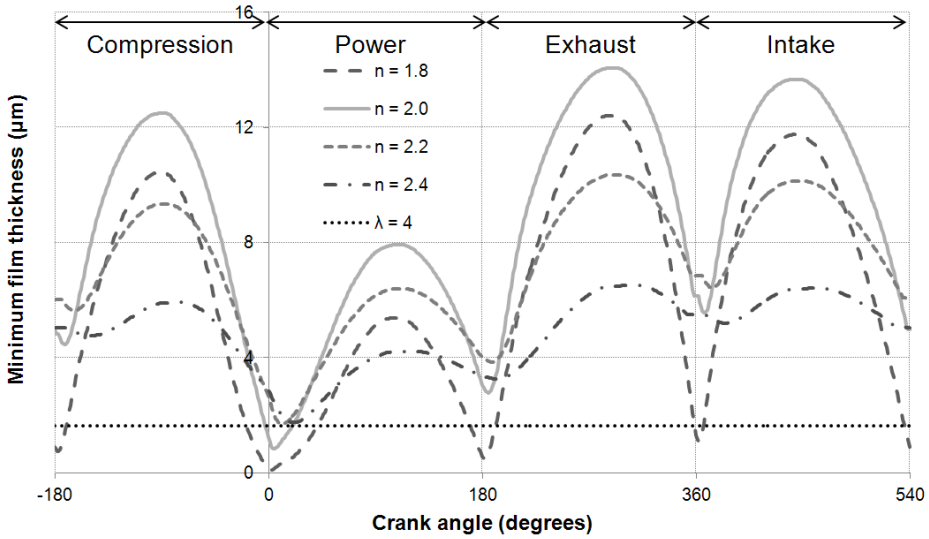

Figure 4: Variations of minimum film thickness for different ring profiles during a typical engine cycle

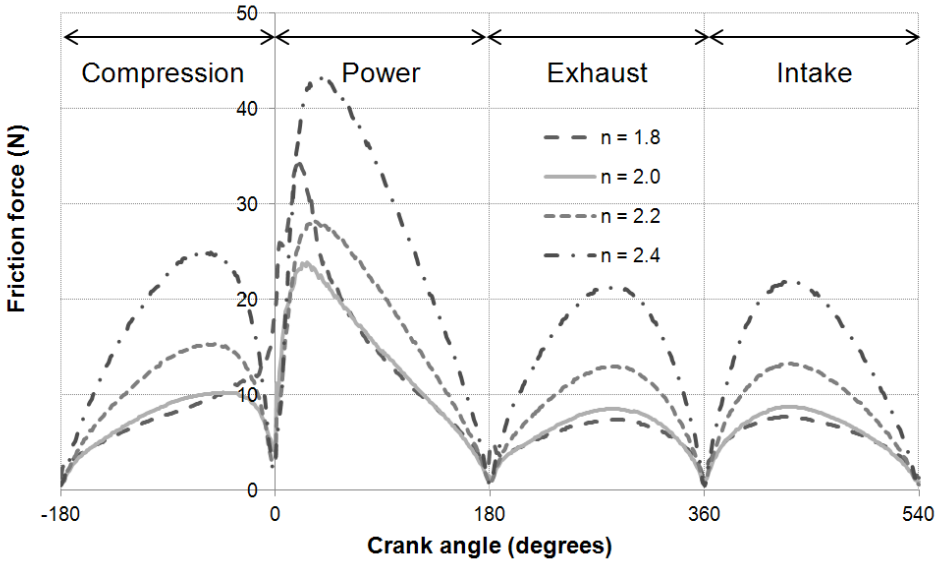

Figure 5: Variations of total friction force for different ring profiles during a typical engine cycle

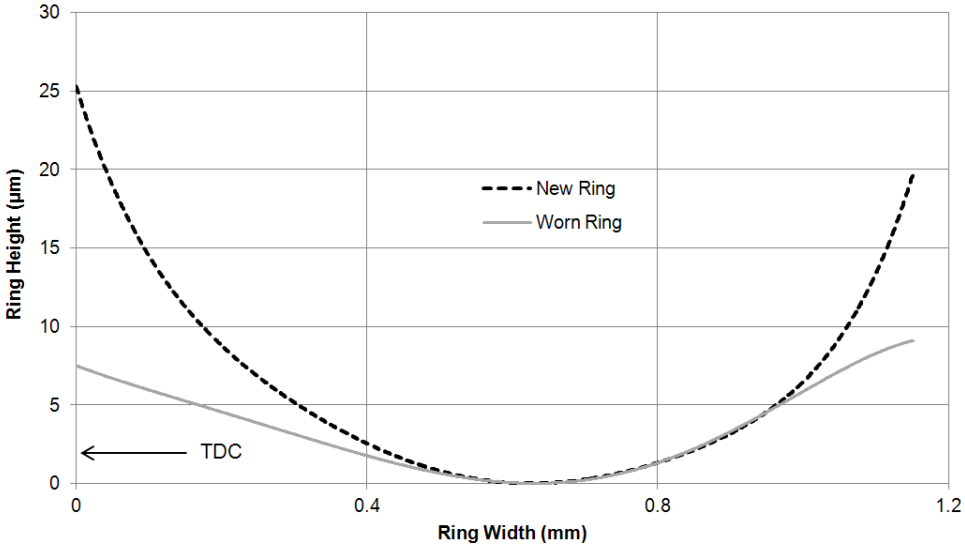

Figure 6: Typical new and worn (end of the life cycle) ring profiles

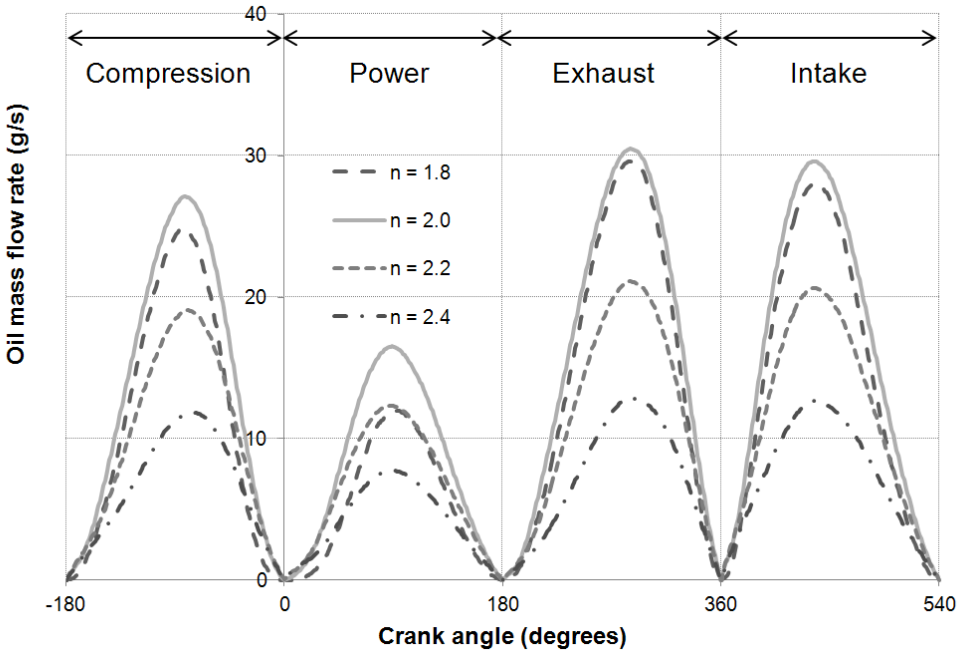

Figure 7: Variations of lubricant mass flow rate for different ring profiles during a typical engine cycle

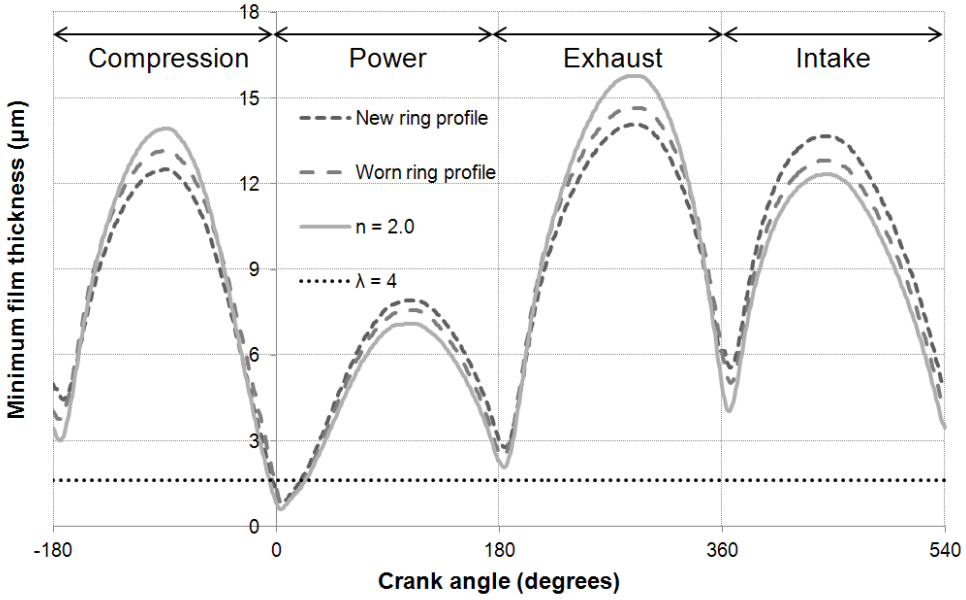

Figure 8: Variation of minimum film thickness for various rings

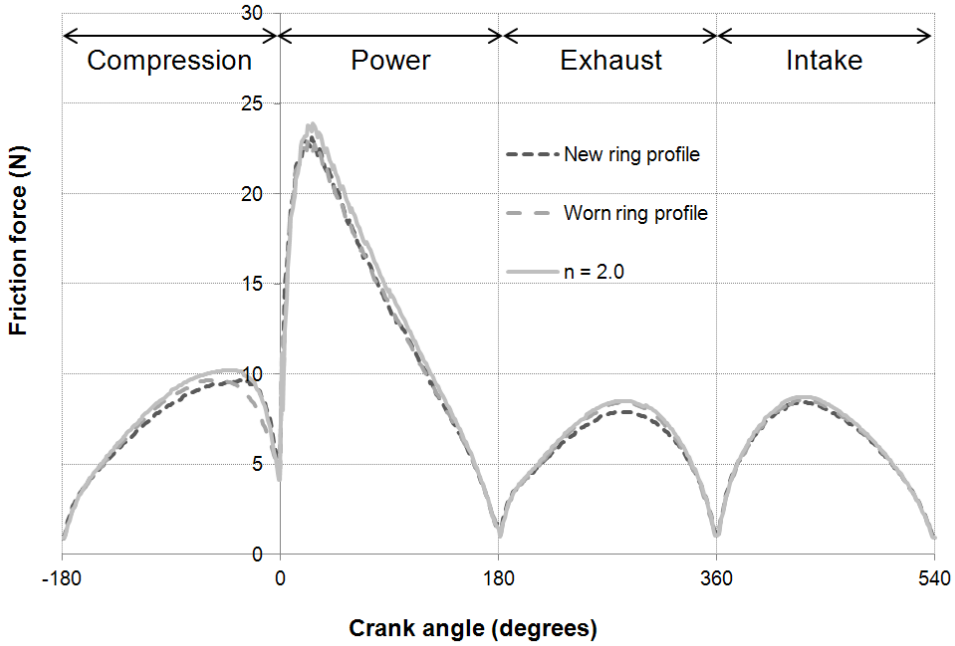

Figure 9: Total viscous and boundary friction based on composite Ra values

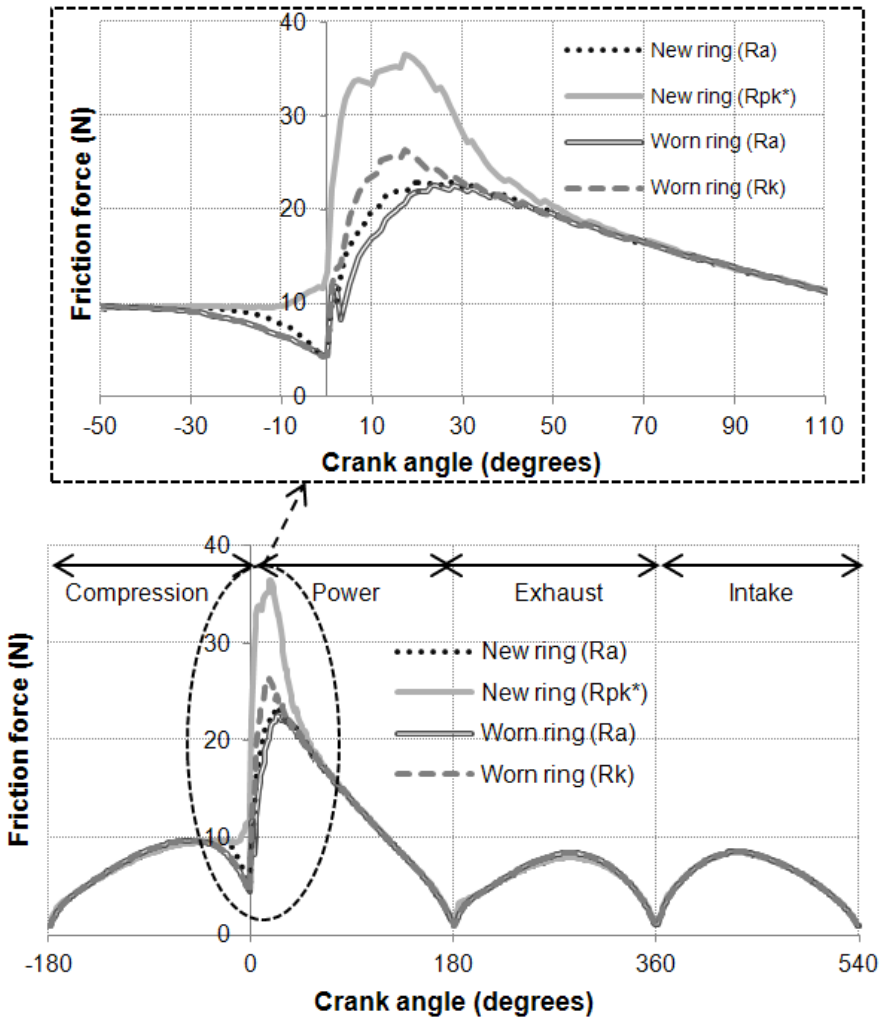

Figure 10: Total friction force: viscous and boundary

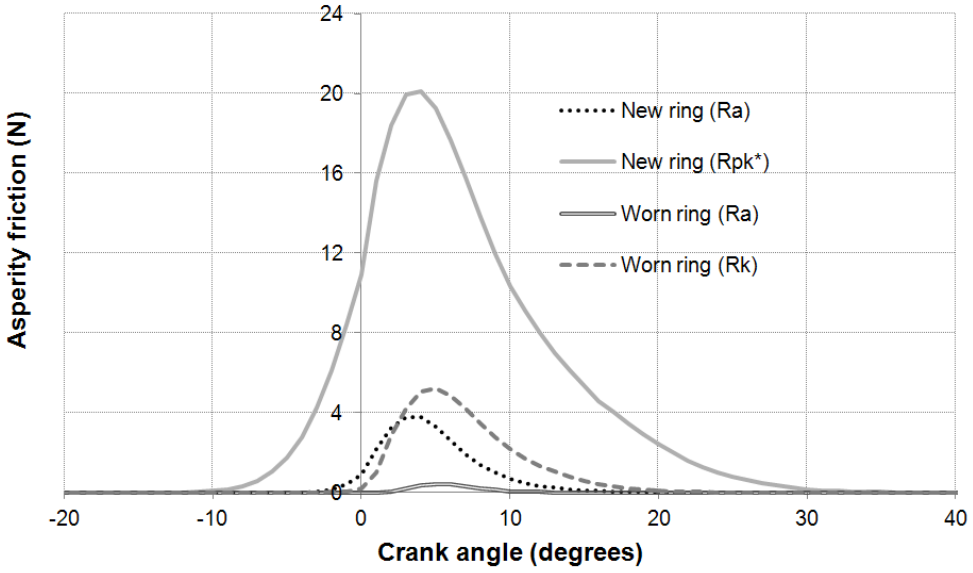

Figure 11: Asperity friction force for near TDC